Multielectron effects in strong-field ionization of CO_2: Impact on differential photoelectron spectra

Vinay Pramod Majety[1,2,*] and Armin Scrinzi[1,†]
[1]*Physics Department, Ludwig Maximilians Universität, 80333 Munich, Germany*
[2]*Max Planck Institute for the Structure and Dynamics of Matter, 22761 Hamburg, Germany*
(Received 3 September 2017; published 21 November 2017)

We report fully differential photoelectron spectra from an *ab initio* coupled-channels treatment of CO_2. Photoionization by laser pulses centered at wavelengths of 400 and 800 nm is considered, with arbitrary molecular alignment and polarization (linear and elliptic). Calculations reveal significant excited-state channel contributions that are, at certain molecular orientations, an order of magnitude larger than the ground-state channel in the rescattering plateau. A partial washout of the multiphoton structure in the above threshold ionization spectra and of the nodal features in angle-resolved spectra is observed due to ionization to excited-state channels. The qualitative nature of the spectra is determined by ionization thresholds, orbital symmetries, and interchannel coupling, in order of precedence.

DOI: 10.1103/PhysRevA.96.053421

I. INTRODUCTION

The advent of intense near-IR laser pulses in the early 1990's led to the discovery of several highly nonlinear phenomena, such as high harmonic generation, high-order above threshold ionization, and nonsequential multiple ionization [1–3]. The last two decades saw various proposals of imaging and spectroscopic techniques based on these phenomena that could deepen our understanding and improve control of atomic-scale phenomena such as chemical reaction mechanisms and solid-state transport phenomena.

In the context of molecular imaging, one of the widely pursued techniques is the laser-induced electron diffraction (LIED) technique [4,5], where the electrons ionized by a laser pulse are redirected back to the source by the same laser field where they scatter off the parent system carrying structural information. The extraction of bond lengths [6–8] and certain dissociation dynamics [9] in small molecules from experimentally measured differential photoelectron spectra has been recently reported. The initial proof-of-principle experiments show promise, but the evolution of these ideas into general techniques would need a deeper understanding of the complex multielectronic and vibrational motion that the strong laser field would induce.

In this paper, we theoretically explore the presence of multielectron effects (within a frozen nuclei approximation), during molecular strong-field ionization, and particularly their impact on photoelectron spectra that would have consequences on LIED imaging. The challenge to an *ab initio* modeling of molecular strong-field ionization (SFI) and computing the associated photoelectron spectra ensues from the high dimensionality of the problem when several electronic degrees of freedom are allowed to respond to the external field, and from the large phase-space requirements needed to describe strong-field ionization, even for a one-electron system. Considerable progress has been made to control the latter problem through the development of the time-dependent surface flux method (t-SURFF) [10,11]. The former challenge, however, remains. Popular choices to handle this many-body problem in the context of photoionization studies include the coupled-channels method [12,13], the R-matrix method [14], variants of the configuration interaction [15,16], and the multiconfigurational time-dependent Hartree-Fock methods [17–21]. Each of these methods cuts down the total Hilbert space to the seemingly essential part needed to describe the ionization process using different protocols.

The application of these methods to the computation of photoelectron spectra in the long-wavelength regime has, however, been minimal so far. Spectra for atoms, using a multielectron theory, have only been recently reported using the R-matrix method [22] and the hybrid antisymmetrized coupled-channels (haCC) method [13]. In the case of molecules, the increased cost of computations resulting from reduced symmetry has rendered such computations infeasible so far. Theoretical modeling has been confined to single-electron approximations and strong-field approximation (SFA) based models [23–26], with the exception of molecular hydrogen [13,27], and the impact of multielectron effects on molecular photoelectron spectra has remained unexplored.

The CO_2 molecule has often been used in the literature as a prototype for nonpolar molecules. It is one of the simplest molecules that exhibits signatures of multielectron effects in various observables associated with strong-field ionization (SFI). In a seminal work by Smirnova and co-workers [28], the relevance of inner orbital ionization and channel coupling in the high harmonic spectroscopy of CO_2 was demonstrated. In Ref. [29], again using CO_2 as an example, the role of the exchange interaction in SFI was demonstrated by the authors. We report here the fully differential photoelectron spectra for CO_2 molecule in the low-frequency regime, obtained from a multielectron approach, and analyze the nature of the multielectron effects involved. We use the hybrid antisymmetrized coupled-channels treatment of the molecular electronic structure presented in Ref. [13] and established in Refs. [29,30] with the t-SURFF to compute fully differential (angle- and channel-resolved) photoelectron spectra. Spectra are computed with linear as well as elliptically polarized ionizing fields.

The fully differential photoelectron spectra presented here reveal significant excited ionization channel contributions in

*vinay-pramod.majety@mpsd.mpg.de
†armin.scrinzi@lmu.de

consonance with the earlier findings on the importance of inner orbital ionization [28]. In addition, these excited-state channels dominate in the rescattering region depending on the molecular orientation with respect to the laser polarization (defined by an angle, say, α). For example, when $\alpha = 90^\circ$, the highest occupied molecular orbital (HOMO)-1 channel dominates the HOMO channel by an order of magnitude in the rescattering region. This opens up the possibility to image channel-specific dynamics in LIED experiments by choosing a specific molecular orientation. Other consequences of multiple orbital ionization include washout of the multiphoton peak structure in certain photoelectron electron energy windows and of the nodal features in the total angle-resolved photoelectron spectra. An ionic channel analysis of the spectra and its comparison with the corresponding single-channel calculations reveal that the spectra are qualitatively determined by the ionization thresholds, orbital symmetries, and interchannel couplings, in order of precedence.

We present the computational methodology in brief in Sec. II and discuss the results in Sec. III.

II. COMPUTATIONAL METHOD

The molecular time-dependent Schrödinger equation is solved within the frozen nuclei approximation with the following basis expansion for the electronic wave function,

$$|\Psi\rangle = \sum_{i,\mathcal{I}} \mathcal{A}|i\rangle|\mathcal{I}\rangle C_{i,\mathcal{I}}(t) + |\mathcal{G}\rangle C_{\mathcal{G}}(t). \tag{1}$$

Here, $\mathcal{A}$ indicates antisymmetrization, $|\mathcal{I}\rangle$ is a set of singly charged cationic states, $|\mathcal{G}\rangle$ is the ground state of the neutral, $|i\rangle$ is a complete single-electron basis, and $C_{i,\mathcal{I}}(t)$, $C_{\mathcal{G}}(t)$ are time-dependent coefficients corresponding to their respective basis functions. A calculation with lowest I channels is referred to as the "haCC(I)" calculation and degenerate states are counted separately. A summary of the method is provided here, while a detailed description can be found in Ref. [13].

The single-electron basis $|i\rangle$ is a product basis consisting of high-order polynomials on finite elements for the radial coordinates and spherical harmonics based on the origin for the angular coordinates. The ionic and the neutral states are computed using the multireference configuration interaction singles doubles method implemented in the COLUMBUS quantum chemistry package [31] using an atom-centered Gaussian basis set (minimally augmented cc-pvtz basis) at the starting point. The choice implies that the multicentered nature of the initial state and the residual ionic states is represented accurately with the Gaussians, leaving only the single continuum to be described by $|i\rangle$. As a result, the angular momentum requirements in the single center expansion $|i\rangle$ remain on par with a corresponding atomic case. On a 25 a.u. simulation volume, we obtain angle-integrated photoelectron spectra that have a relative accuracy of about 10% with respect to radial basis parameters and angular momenta with 50 radial functions constructed from order 10 polynomials and with 35 angular momenta.

We considered a CO_2 molecule frozen at an equilibrium configuration with a C-O bond length of 116.3 pm and the single cationic states $X^2\Pi_g$, $A^2\Pi_u$, $B^2\Sigma_u^+$, $C^2\Sigma_g^+$, and $D^2\Pi_u$

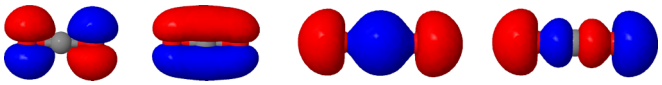

FIG. 1. Isosurfaces of the highest occupied molecular orbital (HOMO), HOMO-1, HOMO-2, and HOMO-3 ordered from left to right, plotted with JMOL software [33] using the Hartree-Fock output of our COLUMBUS calculations.

states with vertical binding energies of 13.68 (13.78,13.77), 17.74 (17.59,17.72), 18.46 (18.08,18.28), 19.74 (19.4,19.48), and 25.47 (22.7,24.19) eV, respectively, with respect to $|\mathcal{G}\rangle$. The values in parentheses are the experimental (first) and theoretical (second), as reported in Ref. [32]. The first few highest occupied molecular orbitals on which the configuration interaction (CI) states are based on are shown in Fig. 1 as a reference to the orbital symmetries needed to analyze our results.

When diagonalizing with the coupled-channels basis, the ground state improves and the thresholds increase. The first ionization potential varies from 13.7 to 13.88 eV between the smallest to the largest coupled-channels basis considered here. The change in the ionization potential (IP) between various haCC calculations is $\leqslant 12\%$ of the photon energies considered. Hence, the possibility for the order of the multiphoton ionization process to change due to the shift in the IP is minimal. Ionization by tunneling is highly sensitive to the IP. An estimate using the molecular tunneling ionization model, MO-ADK [34], suitable under the quasistatic limit shows that the ionization rates would change on the scale of 20% for a change in the IP by 0.18 eV. This is within the relative accuracy of the spectra that we aim for here. Other examples where IP is crucial would be processes involving resonances. We do not deal with such processes here.

The ionizing field is approximated to have a $\cos^2$, $\cos^8$ envelopes for linearly and elliptically ($\epsilon = 0.87$) polarized fields, respectively. In both cases, we consider three-cycle pulses with central wavelengths of 400 and 800 nm. The peak intensities were chosen to be 10^{14} W/cm^2 in the linear case and 1.76×10^{14} W/cm^2 in the elliptic case. This sets the peak field strengths to the same value in both cases. The molecular axis is fixed to be along the z axis. With linear polarization, polarization directions parallel ($\alpha = 0^\circ$), perpendicular ($\alpha = 90^\circ$), and at 45° with respect to the molecular axis are considered. In the elliptic case, fields in the plane parallel and perpendicular to the molecular axis are considered. The exact forms for the vector potentials are

$$A(t) = A_0 \cos^2\left(\frac{\pi t}{2N_c T}\right) \sin(\omega t)\hat{p} \tag{2}$$

and

$$A(t) = \frac{A_0}{\sqrt{1+\epsilon^2}} \cos^8\left(\frac{\pi t}{4N_c T}\right) \times \left[\sin\left(\frac{2\pi t}{T}\right)\hat{e}_1 + \epsilon \cos\left(\frac{2\pi t}{T}\right)\hat{e}_2\right], \tag{3}$$

where A_0 is the vector potential at the peak field, T is the duration of the optical cycle at the respective wavelength, ϵ is the measure of the ellipticity, N_c is the number of cycles, and

$\hat{p},\hat{e}_1,\hat{e}_2$ are unit vectors that define the polarization. When the field is in the XZ plane, $(\hat{e}_1,\hat{e}_2) = (\hat{z},\hat{x})$, and when in the XY plane, $(\hat{e}_1,\hat{e}_2) = (\hat{y},\hat{x})$.

The nonperturbative external laser field is treated classically in the dipole approximation and the wave function is discretized in a mixed gauge representation. A length gauge representation is used in the region encompassing the ionic, neutral states, and a velocity gauge representation thereafter. The specific gauge choice is motivated by our earlier findings on its efficiency [35]. The time propagation is done with the classical fourth-order Runge-Kutta method and the absorbing boundary conditions are imposed using the infinite-range exterior complex scaling scheme [36].

Fully differential photoelectron spectra are computed using the time-dependent surface flux method (t-SURFF) [10,11], where the spectra are computed from the electron flux through a surface [defined by a radius referred to here as the t-SURFF radius (R_c)], instead of a brute force projection of the wave function over the entire volume onto the single continuum, that are, anyway, only approximately known. As a result, the wave function is represented numerically only on a small spherical region where nontrivial dynamics (other than the motion of a free electron) occurs and absorbing boundary conditions are imposed at R_c. Beyond that radius, the dynamics is assumed to follow the Volkov solutions [37] for a free electron in a dipole field. This amounts to truncating all the potentials to zero beyond R_c, and to avoid artifacts caused by the abrupt truncation of the potential, we smoothly truncate the potential using a third-order polynomial over a small region before R_c. The approximation can be controlled by moving the t-SURFF radius outwards and an error estimate can be made.

The truncation affects the Hartree potential and nuclear Coulomb potential whose combination far from the nucleus has a $1/r$ behavior. The exchange potentials, as they involve overlaps with the Gaussian bound orbitals, fall off even more quickly and are not affected by this truncation. (For the matrix elements involved, see Ref. [13].)

In this work, we do not aim for a rigorous convergence with respect to long-range Coulomb truncation. In order to keep the computational requirements under check, we restrict ourselves to a simulation volume of radius 25 a.u. that captures the essential multielectron dynamics.

The largest computations presented here took about 12 days on a standard 16 core machine with 128 GB of memory using our current implementation for shared memory machines.

A. Limitations

The ansatz (1) treats the polarization contribution from the single continuum and multielectron effects such as exchange interactions and channel couplings exactly. But the polarization of the core electrons is not described completely. In principle, a complete description of polarization for all the electrons would need complete continuum space and not just a single continuum. This, however, entails solving the Schrödinger equation in full generality, which is not feasible. Conceptually, one can extend the current formulation to include double-continuum states, but this could not have been attempted so far due to increased computational costs.

A coupled-channels model is a useful tool to study molecular strong-field ionization only when the relevant multielectron effects can be described using a few-channel expansion. One would expect that the current regime of ionization, that is highly nonlinear with respect to the ionization thresholds, would fit into such a case if the core electrons are only "gently" polarized. For obtaining ionization rates, such a description was found to be sufficient [29,30], though it remains to be seen if it holds in the case of a differential quantity such as the photoelectron spectra.

If a large number of highly excited states is required, our model ceases to be suitable. Increasing the number of states beyond the lowest few does not necessarily lead to convergence, as the ionic bound states do not form a complete set. Further, the highly excited states would need to be strongly adjusted to the field in order to maintain any specific physical meaning over an arbitrarily chosen basis. Hence, convergence in a strict sense using a large number of ionic channels is not sought for here. The model can, however, allow us to understand the role of possible multielectron effects by studying the dependence of spectra on the few channels that can be included in practice. In this work, we restrict ourselves to the first six to eight ionic channels.

B. Uncoupled calculations

In order to analyze the nature of multielectron effects that appear in the spectra, we also perform uncoupled single-channel calculations where the wave function is represented as

$$|\Phi_{\mathcal{I}}\rangle = \sum_i \mathcal{A}|i\rangle|\mathcal{I}\rangle C_{i,\mathcal{I}}(t) + |\mathcal{G}\rangle C_{\mathcal{G}}(t). \tag{4}$$

These uncoupled calculations correspond to single-electron calculations when only the Dyson orbital ($\langle\mathcal{I}|\mathcal{G}\rangle$) corresponding to the considered channel $|\mathcal{I}\rangle$ is allowed to ionize. Note that exchange, however, is fully respected, which is different from single-electron calculations in model potentials.

These single-channel functions $\Phi_{\mathcal{I}}$ are only orthogonal asymptotically when one electron is far from the nucleus. Close to the nuclei, they are nonorthogonal. In addition, each calculation contains a neutral ground state which introduces further nonorthogonality. As a consequence, we cannot rigorously consider this as a decomposition into noninteracting channels. Quantitative comparisons, especially for the sum spectra, between uncoupled-channel calculations and full haCC calculations must be treated with caution, due to possible double counting.

C. Observables

Here, we give the explicit forms of the observables presented in the paper. We label the fourfold differential photoelectron spectrum as $\sigma(\mathcal{I},E,\Omega)$, where $\mathcal{I}$ is the residual ionic channel index, E is the energy of the photoelectron, and $\Omega = (\theta,\phi)$ denotes the angles defining the direction of emission. The total integral of this object gives ionization yield Y,

$$Y = \sum_{\mathcal{I}} Y_{\mathcal{I}} = \sum_{\mathcal{I}} \int\int dE\, d\Omega\, \sigma(\mathcal{I},E,\Omega), \tag{5}$$

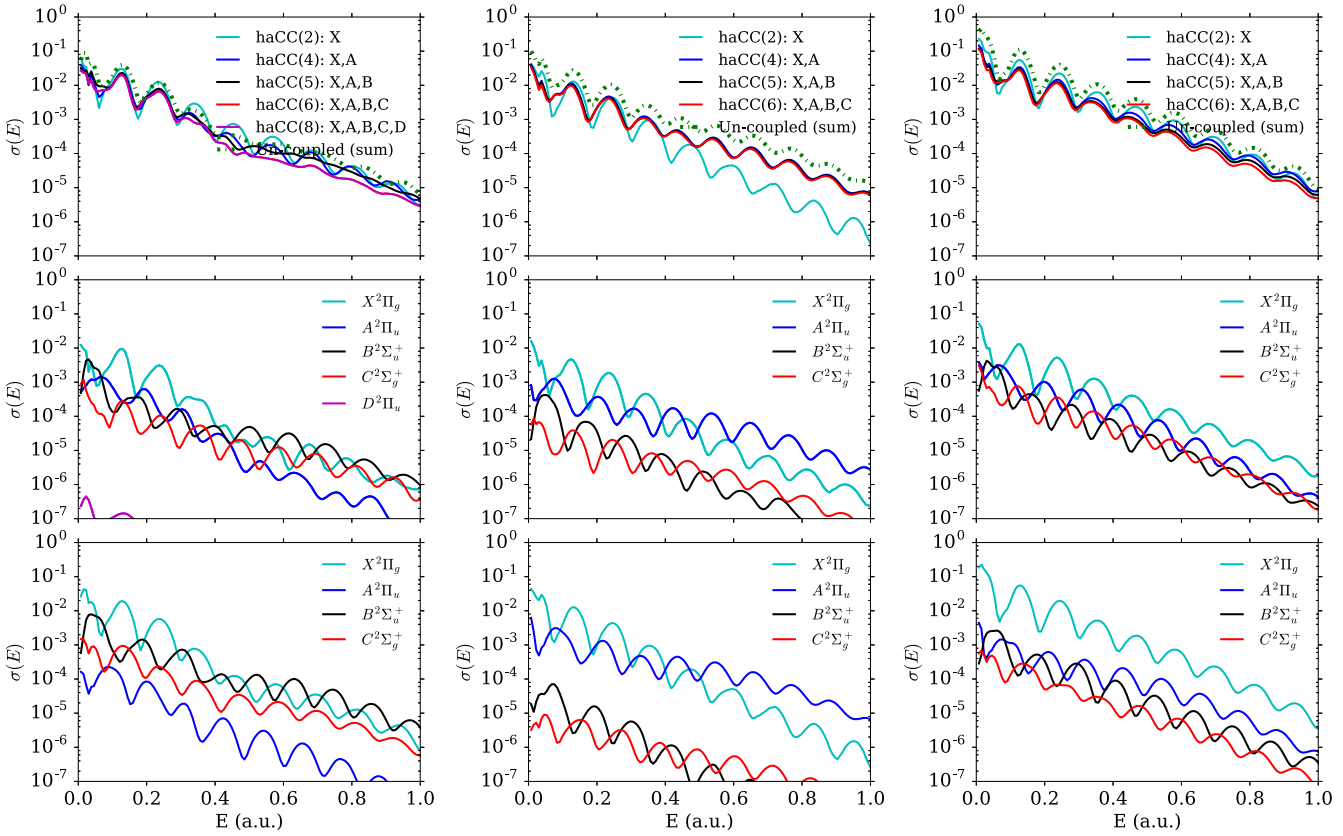

FIG. 2. Single ionization spectra at 400 nm with molecular orientations $\alpha = 0^\circ$ (left column), $\alpha = 90^\circ$ (center column), and $\alpha = 45^\circ$ (right column). Plots in the upper row show spectra from coupled-channels calculations with different numbers of ionic channels and sum spectra from uncoupled-channels calculations. The plots in the second row show an ionic channel analysis of the spectra from the largest haCC calculation, and the plots in the bottom panel show spectra from uncoupled single-channel calculations.

with $Y_{\mathcal{I}}$ being the ionization yield into each residual ionic channel. The energy-resolved spectrum is defined as

$$\sigma(E) = \sum_{\mathcal{I}} \int d\Omega\, \sigma(\mathcal{I}, E, \Omega), \tag{6}$$

and the energy, channel-resolved spectrum is defined as

$$\sigma_{\mathcal{J}}(E) = \int d\Omega\, \sigma(\mathcal{J}, E, \Omega). \tag{7}$$

With arbitrary polarizations, symmetries are lost and hence we present various cuts (in the three-dimensional space) of the angle, energy-resolved spectrum. Such a cut, for example, in the XY plane can be defined as

$$\sigma\left[E, \theta = \frac{\pi}{2}, \phi \in [0 : 2\pi)\right] = \sum_{\mathcal{I}} \sigma(\mathcal{I}, E, \Omega). \tag{8}$$

III. RESULTS

In this section, we present photoelectron spectra from coupled-channels calculations and analyze the nature and relevance of multielectron effects by performing an ionic channel analysis and by comparing with uncoupled single-channel calculations.

A. Linearly polarized ionizing fields

The upper panels of Figs. 2 and 3 show total single ionization spectra as a function of the number of ionic channels in the coupled-channels expansion at 400 and 800 nm, respectively, and with polarization directions defined by angles $\alpha = 0^\circ$, 90°, and 45°.

The largest calculations that were possible with the current implementation are presented in each case. With laser parameters ($\lambda = 400$ nm, $\alpha = 0^\circ$), up to eight channels could be included, with ($\lambda = 800$ nm, $\alpha = 0^\circ$) and ($\lambda = 400$ nm, $\alpha = 90^\circ$,45°) up to six channels, and for the cases of ($\lambda = 800$ nm, $\alpha = 45^\circ$,90°) up to five channels could be included. The largest calculations that could be performed in each case were defined by the duration of the ionizing pulse and the symmetry of the problem. With the exception of the spectra at parameters ($\lambda = 800$ nm, $\alpha = 0^\circ$), the spectra amplitudes [Eq. (6)] from the largest two coupled-channels calculations in each case vary by less than 30%. Based on the impact of the D channel at ($\lambda = 400$ nm, $\alpha = 0^\circ$), one does not expect further changes in the ($\lambda = 800$ nm, $\alpha = 0^\circ$) spectrum.

The spectra exhibit above threshold ionization (ATI) peaks. At 400 nm, the ATI peaks fall off exponentially with the order. At 800 nm, the spectra exhibit the well-known rescattering plateau with characteristic cutoffs around $2U_p$ and $10U_p$ ($U_p \approx 0.22$ a.u.), where U_p is the pondermotive energy. In all of the cases, the spectra change with the inclusion of excited

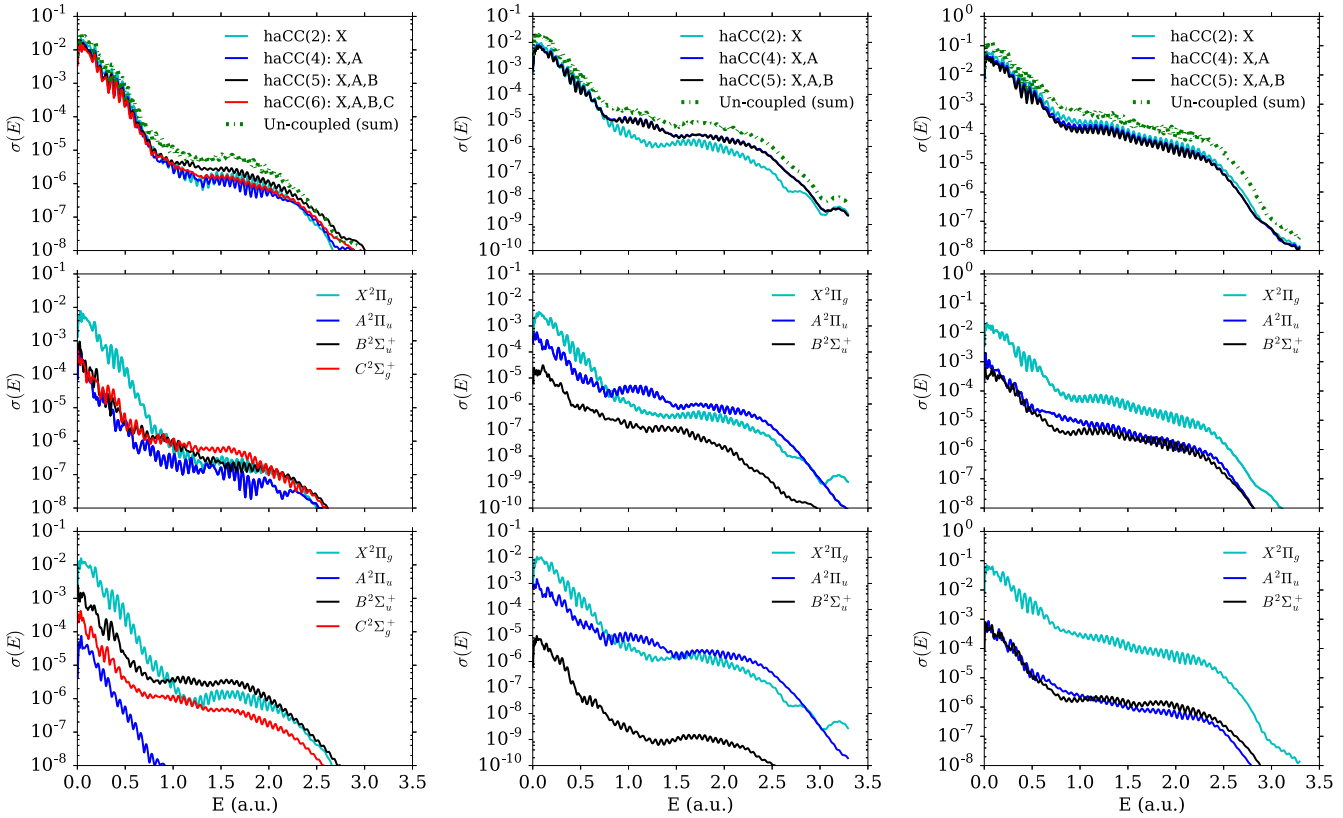

FIG. 3. Single ionization spectra at 800 nm with molecular orientations $\alpha = 0^\circ$ (left column), $\alpha = 90^\circ$ (center column), and $\alpha = 45^\circ$ (right column). Plots in the upper row show spectra from coupled-channels calculations with different numbers of ionic channels and sum spectra from uncoupled-channels calculations. The plots in the second row show an ionic channel analysis of the spectra from the largest haCC calculation, and the plots in the bottom panel show spectra from uncoupled single-channel calculations.

ionic channels, indicating the participation of more than one electron in the ionization process. The total yields decrease when the number of channels is increased. In addition to the improvement in the field-free ground state, the dynamical core electron polarization is better described by the larger channel basis which leads to larger quadratic Stark shifts of the neutral versus the residual ion. Hence, along with the 0.18 eV increase in the field-free ionization potential from haCC(2) to haCC(6), there is an additional increase in the Stark shift of the ground state by about 0.2 eV. The net increase in the ionization potentials leads to a general reduction in ionization probability, as is expected in the current regime of tunnel and multiphoton ionizations (in the absence of any resonances). This is consistent with the findings in Ref. [29], where we presented static field ionization rates. On a qualitative level, one observes the following as the channel basis is enlarged: The changes are minimal when $\alpha = 45^\circ$. When $\alpha = 0^\circ$, a washout of the multiphoton peak structure is observed in the photoelectron energy range 0.4–1.0 a.u. at 400 nm and in the energy range 1–1.5 a.u. at 800 nm. When $\alpha = 90^\circ$, there is a significant enhancement of the yields at higher photoelectron energies.

To better understand the spectral features, we perform an ionic channel analysis and perform uncoupled-channel calculations according to ansatz (4). The corresponding results for each case are presented in the second and third rows of Figs. 2 and 3. The sum of the uncoupled-channel calculations is presented in the top panels. Qualitatively, the sum of the uncoupled spectra agrees with the full haCC spectrum, but consistently exceeds it. This might be attributed to the absence of any multielectron Stark shift. However, a rigorous discussion would require ruling out any double counting due to the nonorthogonality of the uncoupled channels.

An ionic channel analysis reveals that the contribution of excited channels to the total ionization yield in all considered cases is on the scale of 5%–10%, indicating that they must be considered for any careful analysis. While at $\alpha = 45^\circ$, the ground-state channel dominates at all photoelectron energies, at $\alpha = 0^\circ$, the B,C states, and at $\alpha = 90^\circ$, the A state dominate at higher photoelectron energies. The washout of the multiphoton peak structure occurs as several ionic channels contribute on a similar level at the concerned photoelectron energies and the ionization thresholds that vary by only a few eV cause different offsets of the multiphoton peaks in the various channels.

This unexpected dominance of the excited ionization channels at higher photoelectron energies is a result of the symmetry of molecular orbitals: the interplay of the nodal planes and the electron density. At 800 nm, the three-step classical model [38] can be employed to understand the enhancement of excited states in the plateau region which has been well established as a signature of rescattering. This is further supported by the absence of a plateau structure with elliptically polarized fields presented in the next section. When $\alpha = 90^\circ$, the A

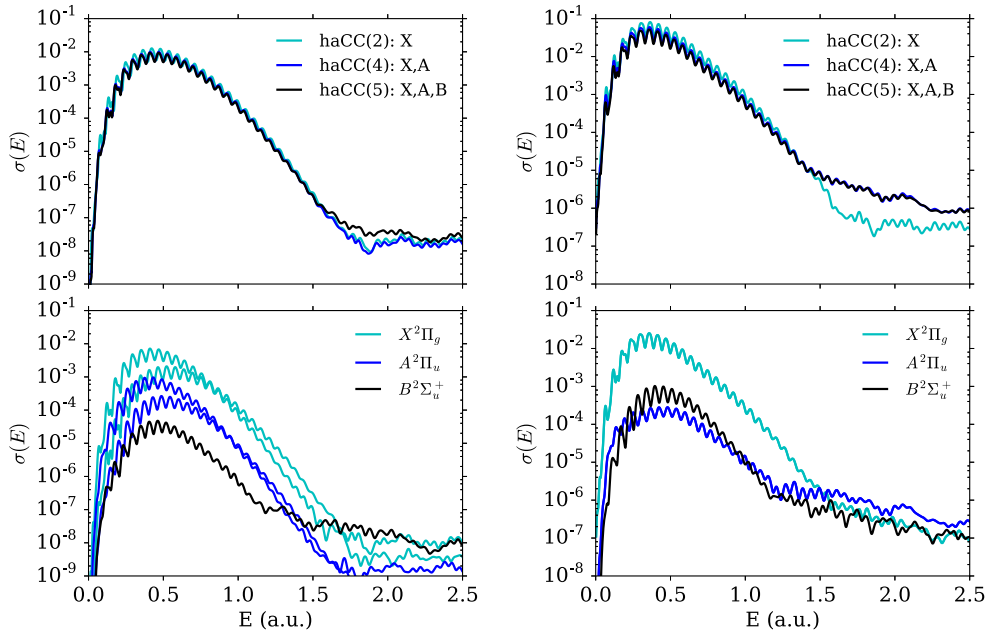

FIG. 4. Single ionization spectra at 800 nm with elliptic polarization in the XY (left) and XZ (right) planes. Plots in the upper row show spectra from coupled-channels calculations with different numbers of ionic channels. The plots in the lower row show an ionic channel analysis of the spectra from the largest haCC calculation. When the ionizing field is in the XY plane, the symmetry of the Π states is broken and the ionization contributions differ, as indicated by curves of the same color.

channel dominates as the ground-state X channel has a node in the polarization plane in which rescattering occurs, whereas when $\alpha = 0^\circ$, both X and A channels are suppressed and ionization to the B,C channels become important. Since the ionization threshold to different channels only differs by a few eV, suppression of ionization to a specific channel for symmetry reasons uncovers contributions to ionization to excited-state channels. At 400 nm, the separation of ionization into tunneling and recollision loses validity and these pictures cannot be applied uncritically. The similarity of the slopes of the channel-resolved spectra and the uncoupled single-channel spectra indicates that the behavior can be attributed to the nature of the ionizing orbital that determines the multiphoton ionization cross sections and thereby the slope of the curves.

The uncoupled single-channel calculations, qualitatively, are similar to the channel-resolved spectra at $\alpha = 45^\circ$ and $\alpha = 90^\circ$. This indicates that ionization at these parameters can qualitatively be considered as largely independent ionization into the individual channels. At $\alpha = 0^\circ$, however, the relative contributions of the B,C channels in the coupled-channels calculation versus uncoupled single-channel calculations differ. This effect is more striking at 800 nm as compared to the 400-nm case. Both states share the same nodal structure and are energetically separated by about 1 eV. In the uncoupled calculation, the lower-lying C state contributes less, while in fully coupled haCC(6), C dominates over B at higher photoelectron energies. This can be attributed to interchannel coupling.

B. Elliptically polarized ionizing field

The upper panels of Fig. 4 show total ionization spectra at 800 nm with elliptically polarized ionizing fields in the XY and XZ planes and with the molecular axis along the z axis. The pulses have been chosen to have peak fields in the y and z directions, respectively. The spectra exhibit ATI peaks with an overall peak at about twice the pondermotive energy ($U_p \approx 0.22$ a.u.) and with no rescattering plateau. The channel analysis shows that the contribution of the excited-state channels is about 10% when the field is in the XY plane and about 5% when the field is in the XZ plane. These relative contributions of the excited channels is in accordance with the findings in the previous section with linearly polarized fields. In the XY case, the relevant excited-channel contribution comes from the A state, while in the XZ case, the B channel dominates the A channel. This stems from our choice of peak field direction and orbital symmetry. If the peak field was chosen to be along the X (or Y) axis, the A channel would dominate B in both cases.

C. Angle-resolved spectra

In order to demonstrate the further potential of our method, in Fig. 5 we show angle-resolved spectra summed over all the ionic channels at 800 nm. The spectra are only converged to a relative accuracy of 60% with respect to the single-electron basis ($|i\rangle$) parameters. We briefly mention below the qualitative features arising from symmetry and that are not subjected to the questions of quantitative convergence.

In the case of linear polarization, the cut along the XZ plane is presented. The spectra obtained from a ground-state channel calculation [haCC(2)] exhibit a nodal structure for $\alpha = 0^\circ, 90^\circ$ due to the nodal planes in the highest occupied molecular orbital (HOMO). The contributions from the excited-state channels lead to a washout of the nodal structure. A similar behavior is observed at 400 nm. When $\alpha = 45^\circ$, selective enhancements are seen in the rescattering region, which we

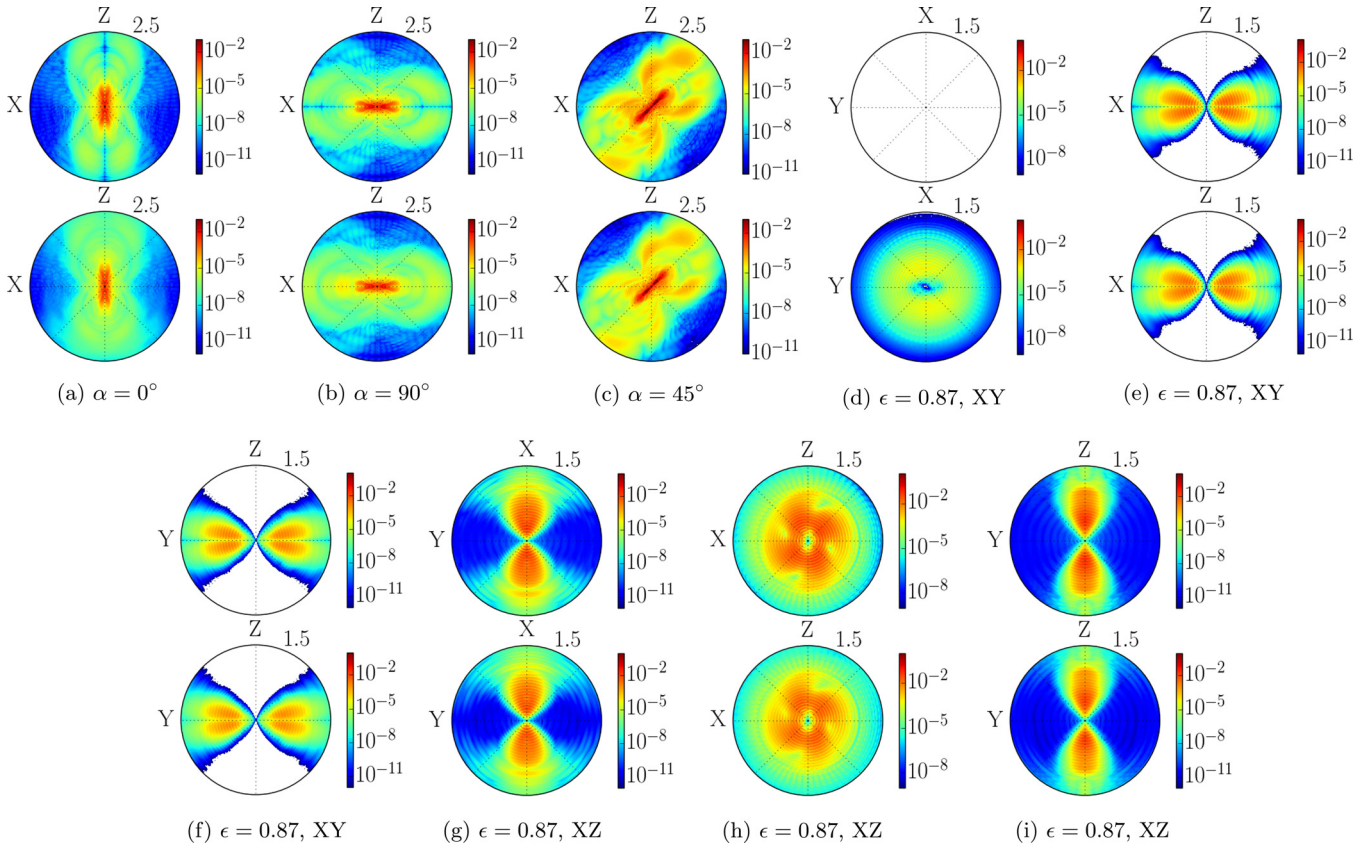

FIG. 5. Cuts of angle, energy-resolved spectra along various coordinate planes at 800 nm. The upper panel of each subplot corresponds to the ground-state calculation (haCC(2)) and the lower corresponds to the largest coupled-channels calculation in each case. The molecular axis is fixed along the Z axis. Subplots (a)–(c) show spectra in the XZ plane with linearly polarized fields with polarization directions that subtend angles of 0°, 90°, and 45° with respect to the Z axis. In the case of elliptic polarization, we show cuts along all the coordinate planes. Subplots (d)–(f) are the spectra when the elliptically polarized field is in the XY plane and (g)–(i) are the spectra when the field is in the XZ plane. The upper panel of (d) is empty, indicating zero emission, and the white regions in (e) and (f) subplots result from masking of the spectral values $<10^{-12}$.

attribute to the structure of HOMO, which is the strongest ionization channel at these parameters.

In the case of elliptic polarization, symmetry along the molecular axis is not present, and we present cuts of the angle, energy-resolved spectra in all the coordinate planes XY, XZ, and YZ. When the field is in the XZ plane, haCC(2) and haCC(5) results are qualitatively similar. The differential spectrum in the XZ plane exhibits a four-lobe structure, reflecting the shape of HOMO. The XY and YZ cuts exhibit a directional emission in the X and Z directions, respectively, reflecting the laser polarization. When the field is in XY plane, the spectra from haCC(2) and haCC(5) are qualitatively similar in the XZ and YZ planes, again with a directional emission in accordance with laser polarization. In the XY plane, however, the haCC(2) calculation shows zero emission resulting from the node in HOMO. When excited channels are included, contributions appear.

Obtaining a better quantitative convergence and an analysis of the interference structures will be a topic of future study.

D. Discussion

Corroborating, it can be concluded that the nature of photoelectron spectra is determined by three factors: ionization thresholds, orbital symmetries, and interchannel coupling, in order of precedence. When the total ionization yield to a specific channel is considered, the ionization threshold is the determining factor. In every example considered, the ground-state channel has the highest yield. When differential spectra are considered, angle-resolved or the rescattering plateau that is sensitive to the wave function in the plane of polarization, orbital symmetries come into the picture. That is, when an energetically favorable channel has a node, the excited-channel contribution becomes important. Finally, when a set of channels is similarly favored by the ionization thresholds and symmetry, interchannel coupling plays a role. This is manifested in the case of $\alpha = 0°$ at 800 nm. We do not observe the X, B channel coupling proposed in the context of high harmonic spectra [28]. A possible explanation would be that the photoelectron spectra and high harmonic spectra present different aspects of strong-field dynamics.

Ionization in the case of linear polarization involves direct ionization along with contributions from recollision, whereas ionization in the elliptic case is purely direct ionization. This is supported by the absence of the plateau feature that is a signature of recollision. Comparing spectra from the linear and elliptic cases, it can be concluded that the excited-channel contributions appear as a result of only the initial tunnel

ionization and recollision plays no role in populating these states. The relative dominance of the excited channels in the plateau region can be attributed to an increase or decrease in the probability for recollision resulting from orbital symmetries.

The knowledge of orbital symmetries combined with molecular alignment technologies can be utilized to selectively populate a particular channel in the rescattering plateau. In the context of the LIED experiments, which aim to extract nuclear dynamics from the rescattering plateau, our results expose the possibility to image channel-specific dynamics. This is, however, subjected to corrections from nuclear motion.

IV. CONCLUSION

We report fully differential photoelectron spectra for a polyatomic molecule using a multielectron description of the molecular wave function. A coupled-channels treatment is used to describe the molecular electronic structure and the time-dependent surface flux method is used to compute the photoelectron spectra. The method is now accessible to studying the strong-field ionization of linear polyatomics with arbitrary polarizations. The ionization of CO_2 by linearly and elliptically polarized laser fields with central wavelengths of 400 and 800 nm was considered.

Our calculations reveal that ionization to excited-state channels is on the order of 5%–10%. While they may be neglected when considering total yields, these states can dominate the ground-state channel at certain momenta or orientations, where the ground-state channel is prohibited for symmetry reasons. This can lead to a host of interesting situations: (1) When considering angle-resolved spectra, the nodal planes one expects from the symmetry of the ground-state channel do not appear. (2) In the momentum-resolved but angle-integrated spectra, specific excited-state channels can dominate in the rescattering plateau region, depending on the molecular orientation. The rescattering process is sensitive to the electron density in the polarization plane, and a nodal plane in the energetically favorable channel leads to the relative dominance of an excited-state channel. When more than one channel becomes similarly favorable by energy and symmetry arguments, their sum can lead to a washout of the ATI structure and also allows the channels to dynamically couple during the ionization process. In the context of the LIED experiments, which aim to extract dynamics from the rescattering plateau, our results with a linear polarization at 800 nm show that one can potentially image channel-specific nuclear dynamics by choosing a particular molecular orientation.

The qualitative nature of the differential spectra are defined by ionization thresholds, symmetries, and channel coupling, in order of precedence. These conclusions would also apply to other small and nonpolar molecules that exhibit bound-state single ionic spectra similar to CO_2.

ACKNOWLEDGMENTS

The authors acknowledge financial support from the German excellence cluster: Munich Advanced Photonics and by the Deutsche Forschungsgemeinschaft under the priority program QUTIF (1840).

[1] P. Agostini and L. F. DiMauro, in *Advances in Atomic, Molecular, and Optical Physics*, edited by E. A. Paul Berman and C. Lin (Academic, New York, 2012), Vol. 61, pp. 117–158.
[2] A. Scrinzi, M. Y. Ivanov, R. Kienberger, and D. M. Villeneuve, J. Phys. B **39**, R1 (2006).
[3] F. Krausz and M. Ivanov, Rev. Mod. Phys. **81**, 163 (2009).
[4] M. Spanner, O. Smirnova, P. B. Corkum, and M. Y. Ivanov, J. Phys. B **37**, L243 (2004).
[5] M. Lein, J. Phys. B **40**, R135 (2007).
[6] M. Meckel, D. Comtois, D. Zeidler, A. Staudte, D. Pavičć, H. C. Bandulet, H. Pépin, J. C. Kieffer, R. Dörner, D. M. Villeneuve, and P. B. Corkum, Science **320**, 1478 (2008).
[7] C. I. Blaga, J. Xu, A. D. DiChiara, E. Sistrunk, K. Zhang, P. Agostini, T. A. Miller, L. F. DiMauro, and C. D. Lin, Nature (London) **483**, 194 (2012).
[8] M. G. Pullen, B. Wolter, A. T. Le, M. Baudisch, M. Sclafani, H. Pires, C. D. Schröter, J. Ullrich, R. Moshammer, T. Pfeifer, C. D. Lin, and J. Biegert, Nat. Commun. **7**, 11922 (2016).
[9] B. Wolter, M. G. Pullen, A.-T. Le, M. Baudisch, K. Doblhoff-Dier, A. Senftleben, M. Hemmer, C. D. Schröter, J. Ullrich, T. Pfeifer, R. Moshammer, S. Gräfe, O. Vendrell, C. D. Lin, and J. Biegert, Science **354**, 308 (2016).
[10] L. Tao and A. Scrinzi, New J. Phys. **14**, 013021 (2012).
[11] A. Scrinzi, New J. Phys. **14**, 085008 (2012).
[12] M. Spanner and S. Patchkovskii, Phys. Rev. A **80**, 063411 (2009).
[13] V. P. Majety, A. Zielinski, and A. Scrinzi, New J. Phys. **17**, 063002 (2015).
[14] M. A. Lysaght, H. W. van der Hart, and P. G. Burke, Phys. Rev. A **79**, 053411 (2009).
[15] L. Greenman, P. J. Ho, S. Pabst, E. Kamarchik, D. A. Mazziotti, and R. Santra, Phys. Rev. A **82**, 023406 (2010).
[16] D. Toffoli and P. Decleva, J. Chem. Theory Comput. **12**, 4996 (2016).
[17] J. Caillat, J. Zanghellini, M. Kitzler, O. Koch, W. Kreuzer, and A. Scrinzi, Phys. Rev. A **71**, 012712 (2005).
[18] D. Hochstuhl and M. Bonitz, Phys. Rev. A **86**, 053424 (2012).
[19] H. Miyagi and L. B. Madsen, Phys. Rev. A **89**, 063416 (2014).
[20] D. J. Haxton and C. W. McCurdy, Phys. Rev. A **91**, 012509 (2015).
[21] T. Sato and K. L. Ishikawa, Phys. Rev. A **91**, 023417 (2015).
[22] O. Hassouneh, S. Law, S. F. C. Shearer, A. C. Brown, and H. W. van der Hart, Phys. Rev. A **91**, 031404 (2015).
[23] N. Suárez, A. Chacón, M. F. Ciappina, B. Wolter, J. Biegert, and M. Lewenstein, Phys. Rev. A **94**, 043423 (2016).
[24] H. Hetzheim, C. Figueira de Morisson Faria, and W. Becker, Phys. Rev. A **76**, 023418 (2007).
[25] M. Busuladžić, A. Gazibegović-Busuladžić, D. B. Milošević, and W. Becker, Phys. Rev. Lett. **100**, 203003 (2008).
[26] K. Liu, K. Renziehausen, and I. Barth, Phys. Rev. A **95**, 063410 (2017).
[27] Y. V. Vanne and A. Saenz, Phys. Rev. A **82**, 011403 (2010).

[28] O. Smirnova, Y. Mairesse, S. Patchkovskii, N. Dudovich, D. Villeneuve, P. Corkum, and M. Y. Ivanov, Nature (London) **460**, 972 (2009).
[29] V. P. Majety and A. Scrinzi, Phys. Rev. Lett. **115**, 103002 (2015).
[30] V. P. Majety and A. Scrinzi, J. Phys. B **48**, 245603 (2015).
[31] H. Lischka, T. Müller, P. G. Szalay, I. Shavitt, R. M. Pitzer, and R. Shepard, WIREs Comput. Mol. Sci. **1**, 191 (2011).
[32] M. Ehara and H. Nakatsuji, Spectrochim. Acta, Part A **55**, 487 (1999).
[33] http://www.jmol.org/.
[34] X. M. Tong, Z. X. Zhao, and C. D. Lin, Phys. Rev. A **66**, 033402 (2002).
[35] V. P. Majety, A. Zielinski, and A. Scrinzi, J. Phys. B **48**, 025601 (2015).
[36] A. Scrinzi, Phys. Rev. A **81**, 053845 (2010).
[37] A. Zielinski, V. P. Majety, and A. Scrinzi, Phys. Rev. A **93**, 023406 (2016).
[38] P. B. Corkum, Phys. Rev. Lett. **71**, 1994 (1993).